Beam modelling and hardware design of an imaging heavy ion beam probe for ASDEX Upgrade

G. Birkenmeier,[a,b,1] **J. Galdon-Quiroga,**[a] **V. Olevskaia,**[a,b] **M. Sochor,**[a] **K. Kaunert,**[a] **G. Anda,**[c] **D. Nagy,**[c] **S. Zoletnik,**[c] **A. Herrmann,**[a] **V. Rohde,**[a] **E. Wolfrum,**[a] **K. Bald,**[a] **J.F. Rivero-Rodriguez,**[d,e] **E. Viezzer,**[d,e] **M. Garcia-Munoz,**[d,e] **and the ASDEX Upgrade Team**

[a] *Max Planck Institute for Plasma Physics, Boltzmannstr. 2, 85748 Garching, Germany*

[b] *Physics Department E28, Technical University Munich, James-Franck-Str. 1, 85748 Garching, Germany*

[c] *Wigner RCP, EURATOM Association HAS, P.O. Box 49, Budapest H-1525, Hungary*

[e] *Department of Atomic, Molecular and Nuclear Physics, University of Seville, 41012 Seville, Spain*

[d] *Centro Nacional de Aceleradores (CNA), Universidad de Sevilla, Junta de Andalucia, Consejo Superior de Investigaciones Cientificas (CSIC), Parque Cientifico y Tecnologico Cartuja, C/ Thomas Alva Edison 7, 41092 Seville, Spain*

E-mail: Gregor.Birkenmeier@ipp.mpg.de

[1] Corresponding author.

ABSTRACT: The imaging heavy ion beam probe (i-HIBP) developed at the ASDEX Upgrade tokamak is a new diagnostic concept for investigations at the edge of high temperature plasmas. By means of a heavy alkali beam injector, a neutral primary beam of an energy of 70 keV is injected into the fusion plasma, where it is ionized generating a fan of secondary beams. These are deflected by the magnetic field of the tokamak and intersect a scintillator plate in the limiter shadow of the tokamak. The light pattern on the scintillator detected with a high speed camera contains radial information on the density, electrostatic potential and the magnetic field in the edge region of the plasma. For the design of the i-HIBP, a detailed beam model including the 3D tokamak magnetic field and beam attenuation effects for cesium and rubidium atoms is developed in order to find the optimum injection scheme within the limited space of the tokamak environment for maximum signal intensities. Based on the optimized injection, the arrangement of the injector outside the vacuum-vessel and the detailed design of the optical in-vessel system is determined.

1 Introduction

For decades, heavy ion beam probes (HIBP) have been used at different experiments for physics investigations of magnetized plasmas [1–5]. HIBPs have the unique capability to measure the electrostatic potential even in the core of the plasma [6], and due to their capabilities to measure fluctuations of electrostatic potential [7, 8], density [9] and magnetic field [10], they are likewise used for turbulence studies . Similar to a classical HIBP, the imaging heavy ion beam probe (i-HIBP) developed for the ASDEX Upgrade tokamak (AUG) [11] deduces information about the plasma from an outgoing heavy ion beam. But it differs from a classical HIBP due to the use of a neutral primary beam and a compact in-vessel ion detector based on a scintillator. For the production of a neutral heavy atomic beam, an alkali beam injector developed for beam emission spectroscopy applications by the Wigner Research Institute, Budapest, is used [12]. The ion detection involving a scintillator and a fast camera is a widely applied concept for fast ion loss detectors [13]. With this components the i-HIBP is based on well developed technologies and more compact than classical HIBPs. It is therefore very similar to the atomic beam probe concept realized at the COMPASS tokamak [14]. In comparison to electrical multi-cell array detectors [10, 14], which are able to directly measure the ion current without introducing additional complications of an optical conversion, the use of a scintillator with an optical detector system has the advantage of a high spatial resolution just limited by the grain size of the scintillator material or the resolution of the optical system while keeping the ability to measure signals down to a few 100 pA/mm^2 due to the amplification effect of the scintillator [15].

The basic principle of the i-HIBP is shown in figure 1 on the left. A neutral atomic primary beam is injected into the plasma where it is ionized by collisions with plasma particles. The ionization along the primary beam generates a fan of ionized secondary beams, which are deflected due to the Lorentz force they experience in the toroidal field of the tokamak. A scintillator detector placed in the limiter shadow collects the secondary beams, and wherever these ions hit the scintillator, photons are emitted giving rise to an elongated light pattern on the scintillator as shown on the right hand side of figure 1. The light pattern is detected with a fast camera and contains information from different radial regions of the plasma: upper parts of the image correspond to regions further inside the plasma and lower parts to regions further radially outward according to the trajectories of the secondary beams. While the *intensity* of the light pattern is determined by the plasma density as well as the electron and ion temperatures, the particular *location* and *shape* of the light pattern is determined by the magnetic field and the electrostatic potential. As shown in ref. [11], magnetic field perturbations δB lead to an offset of the whole light pattern, whereas an electrostatic potential perturbation $\delta\phi$ deflects the light pattern only locally. This way magnetic perturbations can be discriminated from electrostatic potential perturbations. A numerical study of the i-HIBP concept [11] revealed a reasonable measurement resolution for the quantities of interest, but for the hardware design and the real implementation of the i-HIBP, a more detailed investigation under the given spatial restrictions of the AUG experimental set-up is employed. First, an optimum injection geometry and scintillator position has to be found where the signal amplitudes are maximized for a wide range of plasma parameters. For this purpose a detailed beam model is developed as described in section 2. Based on the determined injection geometry, the hardware set-up for the injector and the scintillator-based detector head is designed as detailed in section 4.

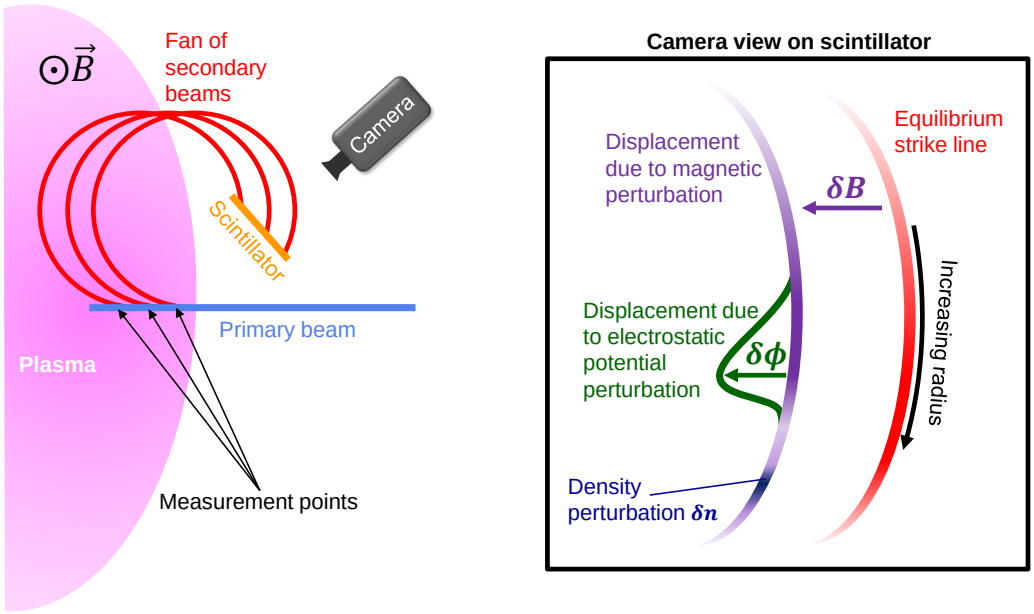

Figure 1. The diagnostic principle of the i-HIBP (left) and the schematic picture of the light pattern on the scintillator as viewed with a camera (right).

2 Beam Modelling

For the two ports available for injection and detection at AUG, the ion flux on the scintillator has to be maximized as a function of the following parameters: toroidal and poloidal injection angle of the primary beam, Cs or Rb beam with an energy up to 100 kV, scintillator position and orientation. Constraints are given by space limitations due to existing hardware inside and outside the vacuum vessel, and, in addition, the injection scheme should allow for measurements at different magnetic fields in the range of 1.8 T and 3.0 T in order to measure in as much as possible plasma scenarios. For the optimization, the 3D version of the particle tracer software FIOS [11] is used, which solves the equation of motion of a charged particle in given magnetic and electrostatic fields. It turned out that the magnetic ripple of the tokamak has to be taken into account, since its effect is of the same order as the expected deflection due to the magnetic field fluctuations which have to be resolved.

For the correct prediction of the ion flux on the scintillator, a quantitative collisional model is developed in order to describe the generation of secondary beams and their attenuation on the way

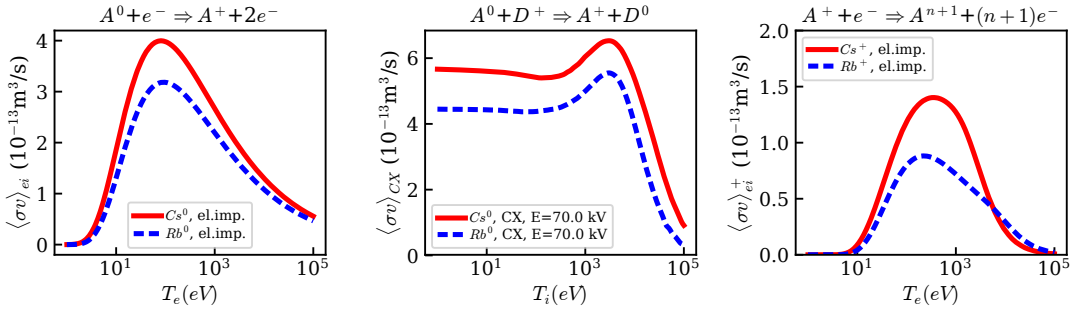

Figure 2. Rate coefficients for the atomic species $A = Cs$ and $A = Rb$. Left: electron impact ionization of neutral atom. Middle: Charge-exchange collisions with Deuterium. Right: electron impact ionization of singly ionized ion.

out of the plasma towards the scintillator. If the primary beam is injected from the outside with a current density $j_p(l = 0)$ and a velocity v_b along the beam coordinate l, it will be attenuated due to collisions in a plasma with electron density n_e, ion density n_i, electron temperature T_e and ion temperature T_i at the position l_0 according to

$$j_p(l_0) = j_p(0) \exp\left\{-\frac{1}{v_b}\int_0^{l_0} \left(n_e \langle\sigma v\rangle_{ei} + n_i \langle\sigma v\rangle_{CX}\right) dl\right\}. \tag{2.1}$$

For the rate coefficient of the electron impact ionization

$$\langle\sigma v\rangle_{ei} \approx 4\pi \int_0^{\infty} \sigma_{ei}(v_e) f_M(T_e) v_e^3 dv_e \tag{2.2}$$

the Lotz formula [16] is used for the cross-section σ_{ei} and an isotropic Maxwell-Boltzmann distribution $f_M(T_e)$ is assumed for the electrons with velocity v_e. These rate coefficients depend on the plasma temperature and are shown for Cs and Rb in figure 2, left.

For Cs and Rb, the charge-exchange collision rates with deuterium (figure 2, center) are in the same order as the electron impact ionization. Since the beam velocity v_b is of the same order as the

most probable deuteron velocities v_i, the three-dimensional integral

$$\langle \sigma v \rangle_{CX} = \int_{\infty}^{\infty} \int_{\infty}^{\infty} \int_{\infty}^{\infty} |\mathbf{v_b} - \mathbf{v_i}| \sigma_{CX}(|\mathbf{v_b} - \mathbf{v_i}|) f_M^{3D}(T_i) d\mathbf{v_i} \tag{2.3}$$

with the three-dimensional Maxwell-Boltzmann distribution for the deuterons $f^{3D}(T_i)$ has to be solved. For Cs a combination of the cross-sections for low [17] and high energy [18] is used, in order to cover a wide energy range. For Rb a combination of data from refs. [19] and [20] are taken.

This data is also needed for the birth profile of the secondary beams along the primary beam coordinate l, which can be described as the current density

$$\Delta j_b(l_0) = j_p(l_0) \left(n_e \langle \sigma v \rangle_{ei} + n_i \langle \sigma v \rangle_{CX} \right) \Delta l \frac{1}{v_b} \tag{2.4}$$

generated in a small volume of the primary beam with length Δl.

The current density $j_s(s)$ along the secondary trajectory coordinate s is determined by the attenuation of the curved secondary beam due to ionization collisions into higher charge states of the ion beam on the way out of the plasma. At the scintillator position s_0 we find

$$j_s(s_0) = \Delta j_b(l_0) \exp\left\{ -\frac{1}{v_b} \int_0^{s_0} n_e \langle \sigma v \rangle_{ei}^{+} \, ds \right\}. \tag{2.5}$$

The rate coefficient $\langle \sigma v \rangle_{ei}^{+}$ is calculated according to formula 2.2, but with the data of the cross sections for secondary ionization as described in ref. [21] for Cs (ionization into all higher states up to Cs^{5+} are taken into account) and ref. [22] for Rb. The rate coefficients for the secondary ionization are shown in figure 2, right.

Figure 3 shows the different contributions to the final ion flux on the scintillator as described with equations 2.1 to 2.5 for a Cs beam with an injected equivalent current density of 2 A/m^2 at

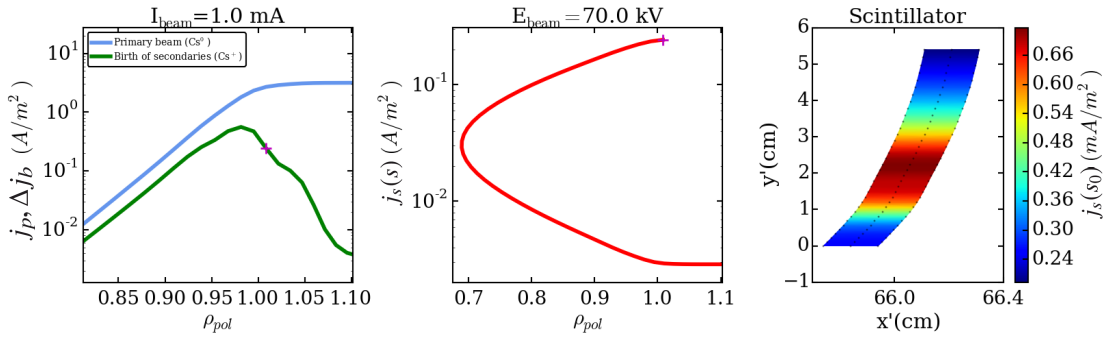

Figure 3. Left: Attenuation of primary beam j_p and birth profile of secondaries Δj_b versus normalized poloidal flux coordinate ρ_{pol}. Middle: Attenuation of secondary beam current density j_s. Right: Ion flux pattern and intensity on scintillator. y' and x' are the vertical and horizontal coordinates on the scintillator plate.

70 kV into a typical L-mode plasma in AUG with a toroidal field of $B_t = 2.5$ T, plasma current of $I_p = 0.6$ MA, an ion and electron temperature at half radius of $T_e = T_i = 700$ eV, and a line-averaged core density of $\bar{n}_e = 2.6 \cdot 10^{19}$ m^{-3}. The equivalent current density of the neutrals of the primary beam is exponentially reduced once it interacts with the plasma particles (figure 3, left). The loss of the primary beam is at the same time the source for the secondary beams. The birth profile of the secondaries, depicted as a radial profile in terms of the normalized poloidal flux coordinate ρ_{pol}, exhibits a maximum slightly inside the last closed flux surface at $\rho_{\mathrm{pol}} = 1.0$. This is a result of the product of the electron density and the rate coefficients (both increasing towards the plasma center) and the available neutral content of the primary beam (decreasing towards the plasma center) according to eq. 2.4. The secondary attenuation (figure 3, middle) is considerable and typically less than 1% of the generated ions of the secondary beams reach the scintillator. Nonetheless, the resulting ion flux on the scintillator of the order of mA/m^2 is sufficient to produce a detectable photon flux of the order of 10^8 to 10^{10} photons/s according to the typical ionoluminescence of the envisaged scintillator material [15].

As can be seen from equation 2.4, the birth rate of secondaries depends on the plasma density, but due to the temperature dependence of the rate coefficients, it is likewise affected by the tem-

peratures. Particularly, due to the strong electron temperature dependence of the electron impact ionization rate coefficient, an intensity perturbation on the scintillator can be related rather to electron pressure perturbations than density perturbations alone in some regions at the edge. Therefore, proper modelling is needed for the correct interpretation of the intensity pattern on the scintillator.

3 Hardware Design

Based on the model described in section 2, an optimum injection scheme in the toroidal sector 13 of AUG was identified. The primary beam is horizontally injected from the outside at the outer midplane of the tokamak tilted by 5° with respect to the major radius of the torus in toroidal direction. The scintillator position is chosen to be about 2.5 cm radially outside of the outermost limiting component with plasma contact. It is vertically placed above the midplane and the orientation of the rectangular shaped scintillator (height: 16.9 cm, width: 6 cm) is chosen almost upright in order to collect the majority of the secondary beam.

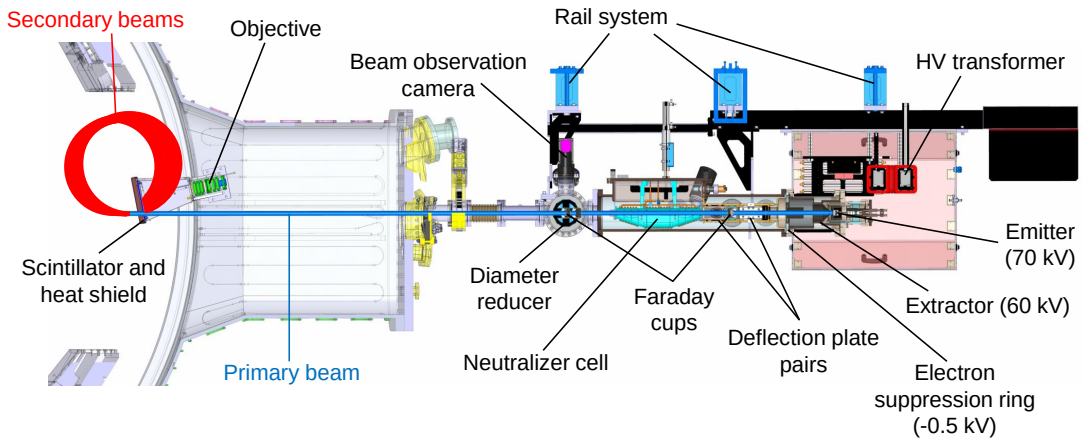

Figure 4. Hardware set-up of the i-HIBP from left to right: Detector head with scintillator and optics, collimator unit, neutralizer, steering plates, accelerator part with ion source.

Based on the chosen injection scheme, the hardware for the whole diagnostic is designed. The main components are shown in figure 4. Outside of the torus vacuum, the alkali beam injector including a beam diagnostics chamber with cameras and Faraday cups on manipulators is placed.

The injector consists of the same components as the injector used for beam emission spectroscopy at the stellarator W7-X [12]. Since the i-HIBP requires, however, higher voltages up to 100 kV, the HV cage is slightly larger than at W7-X for safety reasons. The HV is generated by two HV power supplies with a ripple of 0.1% RMS of the output voltage, which is further reduced by a filter circuit in order to minimize beam energy modulations as necessary to resolve electrostatic potential perturbations in the order of a few tens of Volts. Due to space limitations in the experimental environment of AUG, the whole injector is mounted from the top on a rail system, in order to allow access to other diagnostics by removing the i-HIBP injector during maintenance periods. Between the injector and the torus, a diameter reducer unit is installed. This contains a cylindrical chamber for placing different collimators into the neutral beam line by a rotational mechanism. This is necessary in order to reduce the beam diameter down to 0.25 mm as needed to resolve the small displacements on the scintillator due to potential perturbations in the range of tens of volts [11]. Inside the vacuum vessel, the scintillator is cased in a box with a large aperture at the top, where the secondary beams enter. Towards the plasma a graphite heat shield is placed in order to withstand the thermal loads. A current measurement similar to a Faraday cup setup, a thermocouple and a lamp for in-situ inspection of the scintillator are integrated for monitoring purposes. The light from the scintillator is collected by an objective consisting of six lenses, which focuses the image onto a SCHOTT image guide (not shown in figure 4). This 1700×700 glass fiber bundle guides the image to a fast camera outside the vacuum window.

4 Summary

Based on the beam model described in section 2, an optimal injection scheme for the i-HIBP at AUG was determined in order to achieve ion fluxes on the scintillator up to a few mA/m^2 corresponding to photon fluxes up to 10^{10} into the optical system. With this parameters, the edge region of the plasma

can be accessed with the i-HIBP for a wide range of the toroidal magnetic field from B_t = 1.3 to 2.68 T and plasma current I_p = 0.7 to 1.3 MA of AUG plasmas [23]. The expected measurement sensitivity and spatial resolution of the envisaged i-HIBP system is the same as described in ref. [11] for a slightly different injection scheme. The hardware components of the i-HIBP for AUG were designed based on the optimal injection scheme taking into account the spatial boundary conditions of the tokamak environment. The manufacturing of all components is finished and the assembly in the torus hall ongoing, so that first measurements of the i-HIBP with plasma are expected at the beginning of the AUG campaign 2020.

Acknowledgments

G. Birkenmeier and J. Galdon-Quiroga acknowledge funding from the Helmholtz Association under grant no. VH-NG-1350.

References

[1] P. Schoch et al., *Heavy-ion beam probe diagnostic systems*, *Rev. Sci. Instrum.* **59** (1988) 1646.

[2] T. Crowley et al., *Rensselaer heavy ion beam probe diagnostic methods and techniques*, *IEEE Trans. Plasma Sci.* **22** (1994) 291

[3] Y.N. Dnestrovskij et al., *Development of heavy ion beam probe diagnostics*, *IEEE Trans. Plasma Sci.* **22** (1994) 310

I.S. Bondarenko et al., *Installation of an advanced heavy ion beam diagnostic on the TJ-II stellarator*, *Rev. Sci. Instrum.* **72** (2001) 583

[4] A. Malaquias et al., *Engineering aspects of an advanced heavy ion beam diagnostic for the TJ-II stellarator*, *Proceedings of the 19th Symposium on Fusion Technology 1996, Lisbon, Portugal* (1997) 869

[5] J. A. C. Cabral et al., *The heavy ion beam diagnostic for the tokamak ISTTOK*, *IEEE Trans. Plasma Sci.* **22** (1994) 350

[6] T. Ido et al., *6 MeV heavy ion beam probe on the Large Helical Device*, *Rev. Sci. Instrum.* **77** (2006) 10F523

[7] T. Kobayashi et al., *Spatiotemporal Structures of Edge Limit-Cycle Oscillation before L-to-H Transition in the JFT-2M Tokamak*, *Phys. Rev. Lett.* **111** (2013) 035002.

[8] A.V. Melnikov, *Heavy ion beam probing—diagnostics to study potential and turbulence in toroidal plasmas*, *Nucl. Fusion* **57** (2017) 072004

[9] D.R. Demers et al., *Radial electrostatic flux inferred from core measurements of potential and density fluctuations*, *Phys. Plasmas* **8**, (2001) 1278

[10] A. Malaquias et al., *Evolution of the poloidal magnetic field profile of the ISTTOK plasma followed by heavy ion beam probing*, *Fusion Engineering and Design* **34-35** (1997) 671-674

[11] J. Galdon-Quiroga et al., *Conceptual design of a scintillator based Imaging Heavy Ion Beam Probe for the ASDEX Upgrade tokamak*, *Journal of Instr.* **12** (2017) C08023

[12] G. Anda et al., *Development of a high current 60 keV neutral lithium beam injector for beam emission spectroscopy measurements on fusion experiments*, *Rev. Sci. Instr.* **89** (2018) 013503

[13] M. Garcia-Munoz et al., *Scintillator based detector for fast-ion losses induced by magnetohydrodynamic instabilities in the ASDEX upgrade tokamak*, *Rev. Sci. Instrum.* **80** (2009) 053503

[14] M. Berta et al., *Development of atomic beam probe for tokamaks*, *Fus. Eng. Des*. **88** (2013) 2875

[15] M. Rodriguez-Ramos et al., *First absolute measurements of fast-ion losses in the ASDEX Upgrade tokamak*, *Plasma Phys. Control. Fusion* **59** (2017) 105009

[16] W. Lotz, *Electron-Impact Ionization Cross-Sections and Ionization Rate Coefficients for Atoms and Ions*, *Astrophys. J. Supp.,* **14** (1967) 207

[17] F.W. Meyer, *Single electron capture and loss by H^+, H^0 and H^- in Cs vapour in the energy range 0.1-2.0 keV*, *J. Phys. B: At. Mol. Phys. 13* (1980) 3823

[18] F.W. Meyer and L.W. Anderson, *Charge Exchange Cross Sections for Hydrogen and Deuterium Ions Incident on a Cs Vapor Target*, *Phys. Lett. 54 A* (1975) 333

[19] F. Ebel and E. Salzborn, *Charge transfer of 0.2-5.0 keV protons and hydrogen atoms in sodium-, potassium- and rubidium-vapour targets*, *J. Phys. B: At. Mol. Phys.* **20** (1987) 4531

[20] R.J. Girnius et al., *Charge Exchange Collisions of Deuterium in a Rubidium Vaport Target*, *Nucl. Instr. and Methods* **143** (1977) 505-511

[21] D.R. Hertling et al., *Absolute experimental cross sections for the electron impact single, double, triple, and quadruple ionization of Cs+ ions*, *Journal of Applied Physics* **53** (1982) 5427

[22] M.J. Higgins et al., *Report CLM-R294*, *Culham Laboratory, UK* (1989). Data online available at https://www-amdis.iaea.org/ALADDIN/collision.html

[23] J. Galdon-Quiroga et al., *An imaging heavy ion beam probe diagnostic for the ASDEX Upgrade tokamak*, *Proceedings of the 46th EPS Conference on Plasma Physics 2019, Milan, Italy* (2019) http://ocs.ciemat.es/EPS2019PAP/pdf/P1.1017.pdf